AIAA JOURNAL
Vol. 47, No. 9, September 2009

Accurate Stick Model Development for Static Analysis of Complex Aircraft Wing-Box Structures

Mostafa S. A. Elsayed*
McGill University, Montreal, Quebec H3A 2K6, Canada
Ramin Sedaghati†
Concordia University, Montreal, Quebec H3G 1M8, Canada
and
Mohammed Abdo‡
Bombardier Aerospace, Montreal, Quebec H4S 1Y9, Canada

DOI: 10.2514/1.38447

Aircraft simplified beam finite element models, also known as stick models, are commonly used in aircraft design and multidisciplinary design optimization. Accurate prediction of bending and twisting deformations of the aircraft structure in flight highly depends on the accuracy of the stiffness characteristics in its model. The process of generating a stick model depends on extracting the stiffness properties of the main structure and applying it to a set of beam elements extending along the structure's elastic axis. The present paper proposes a new methodology for extracting accurate bending stiffness properties of an aircraft wing using its 3-D finite element model. The paper reviews the different methodologies commonly used in the industry to generate stick models and gives an insight about the different approximations involved in each methodology and the impact of those approximations on the accuracy of the stick model performance. To validate the proposed methodology, the stick model of the DLR-F6 aircraft wing-box structure is generated using the proposed methodology and also using the methods available in literature. Deformations experienced by the generated stick models are compared with those obtained from the 3-D finite element model of the DLR-F6 aircraft wing box under the same loading condition. The results show that the stick model generated using the proposed methodology is in good agreement with the 3-D finite element model confirming its accuracy.

Nomenclature

A	=	cross-section area, in.^{2}
A_{st}	=	stringer cross-section area, in.^{2}
b_a	=	stringer upper flange width, in.
b_e	=	effective panel width, in.
b_f	=	stringer flange width, in.
b_s	=	stringer pitch, stiffened panel skin width, in.
b_w	=	stringer web width, in.
C	=	correction factor, in.
c_j	=	local chord length at jth wing station, in.
c_s	=	local chord length, in.
D_x, D_y, D_z	=	displacement deformations in x, y, and z directions, respectively, in.
$\mathrm{d}A$	=	infinitesimal area element
$\mathrm{d}F$	=	infinitesimal force component
E	=	modulus of elasticity, lb/in.^{2}
E_{sk}	=	skin modulus of elasticity, lb/in.^{2}
E_{tsk}	=	skin tangent modulus of elasticity, lb/in.^{2}
G	=	modulus of rigidity, lb/in.^{2}
h_s	=	thickness of the wing (thickness of the airfoil), in.
I_x, I_y, I_z	=	second moment of inertia about the x, y, z axes, respectively, in.^{4}
I_{xz}	=	product moment of inertia, in.^{4}
I_y	=	torsional moment of inertia, in.^{4}
I_{x_p}, I_{y_p}, I_{z_p}	=	second moment of inertia about the x_p, y_p and z_p principal axes, respectively, in.^{4}
K_x, K_z	=	area shear factors in the x and z directions, respectively
K_1, K_2	=	area shear factors in the 1 and 2 bending axes directions, respectively
k	=	skin buckling coefficient.
L	=	length of beam element, in.
M_b	=	bending moment, lb · in.
M_x, M_y, M_z	=	moment around general axes x, y and z, respectively, lb · in.
N	=	axial load intensity, lb · in.
s^*	=	wing semispan, in.
t_a	=	thickness of z-stringer upper flange, in.
t_f	=	thickness of z-stringer lower flange, in.
t_s	=	thickness of stiffened panel skin thickness, in.
t_w	=	thickness of z-stringer web, in.
$\bar{X}_i^*$, $\bar{Z}_j^*$	=	x and z coordinates of the centroid of the jth wing station in the wing coordinate system
$\bar{X}_{i,j}^*$, $\bar{Z}_{i,j}^*$	=	x and z coordinates of the ith stringer in the jth wing station in the wing coordinate system
x, y, z	=	general axes
$x_{i,j}$, $y_{i,j}$, $z_{i,j}$	=	axes of the local coordinate system defined to analyze the ith stringer in the jth station.
x_p, y_p, z_p	=	principal axes
x_t, y_t, z_t	=	coordinates of the tip point before deformation
x_t', y_t', z_t'	=	coordinates of the tip point after deformation
x_t'', y_t'', z_t''	=	coordinates of the tip point after deformation in the decoupled system
y_j^*	=	y coordinate of the j station in the wing coordinate system
η	=	plasticity coefficient
η_j	=	normalized wing span coordinate of Jth station
θ_x, θ_y, θ_z	=	deformation rotational angle around the x, y and z axes

Received 7 May 2008; accepted for publication 20 May 2009. Copyright © 2009 by the American Institute of Aeronautics and Astronautics, Inc. All rights reserved. Copies of this paper may be made for personal or internal use, on condition that the copier pay the $10.00 per-copy fee to the Copyright Clearance Center, Inc., 222 Rosewood Drive, Danvers, MA 01923; include the code 0001-1452/09 and $10.00 in correspondence with the CCC.

*Ph.D. Student, Department of Mechanical Engineering, 817 Sherbtooke Street West.
†Associate Professor, Department of Mechanical and Industrial Engineering, 1455 de Maisonneuve Boulevard West. Member AIAA.
‡Engineering Specialist and Flutter and MDO Team Integrator, NCAP Technical and Aerodynamics, 2341 Alfred Nobel, Ville St-Laurent.

$\theta_{x_p}, \theta_{y_p}, \theta_{z_p}$ = deformation rotational angle around the x_p, y_p and z_p-principal axes
σ_{sk} = skin axial stress, lb/in.^{2}
ϕ_x, ϕ_y, ϕ_z = deformation rotational angle around the x, y and z axes of the decoupled system

I. Introduction

DEFORMATIONS of aircraft's structure during flight have a significant effect on the aerodynamic performance of the aircraft. The process of aircraft wing design is multidisciplinary in nature [1–5]. The aerodynamic loads can be used for preliminary sizing of the wing structure. The preliminary dimensions of the wing structure can be used to generate the structural model.

Different levels of structural modeling are presented in Fig. 1. A 3-D finite element model (FEM) is always prepared once the wing's layout and structural details are obtained. The 3-D FEM is commonly used in structural design validation and optimization. Multidisciplinary design optimization (MDO) of an aircraft wing is an iterative process between the structure's discipline represented by its FEM and the aerodynamic discipline. Imposing a complex 3-D FEM in a multidisciplinary iterative process is quite cumbersome and expensive. Alternatively, a simplified lower fidelity beam FEM of the aircraft's structure can be generated and employed in the MDO algorithm. The difficulty is to develop models that are sufficiently simple to be called thousands of times during MDO, but are sophisticated enough to accurately predict wing deformations.

Abdo et al. [6–9] presented two methodologies to create wing stick models of known wing structures. Their methodologies are based on extracting the structural stiffness of the wing with respect to its principal axes. Those stiffness properties are then employed to generate the wing stick model. We see that the limitation of those two methodologies is their dependency on the principal axes as a main condition for extracting high accuracy inertia. Although the process of determining the geometrical principal axes of a structure is straightforward, the complexity of the aircraft wing structure makes this process quite complicated. The stick model is generally created along the wing elastic axis. This applies a geometrical constraint that the stick model principal torsional axis is the wing elastic axis. It is well known that the elastic axis of the wing is tilted from the aircraft wing layout coordinate system due to the dihedral angle, twist of the wing, and the wing sweep. This titling places the bending principal coordinate axes of the stick model in a plane that is tilted from the wing layout coordinate system bending plane. Keeping in mind the taper of the numerous elements of the wing in the spanwise direction makes the process described above a challenge. Alternatively, approximate methods are typically used in the industry to determine those principal axes which, according to our study in the current paper, generate unsatisfactory results.

Other methods are also available in the literature for model reduction. Guyan [10] developed a mathematical methodology for the reduction of the stiffness and mass matrices of a structure to develop the reduced model. A review of [11–14] reveals that the reduced mass and stiffness matrices of the structures do not provide any information about the real physical distribution of the parameters along the real structure. Such distribution is of great importance to check the accuracy of the reduced system. Moreover, although the process of matrix computations is useful in simple structures, using it for complex structures makes the analysis quite expensive. Hashemi-Kia and Toossi [15] developed a technique for reducing airframe FEMs for dynamics analysis and solved some of the problems addressed in [11–14] in which they linked the mass and stiffness characteristics with the physical structure.

The thin walled structural analysis program (TWSAP) is a code developed at Bombardier Aerospace [16]. It calculates sectional properties analytically with respect to the 3-D wing layout coordinate system. The limitation of using the properties generated by the TWSAP is that it constrains the orientation of the stick model elements to be in the structural layout coordinate direction to insure the accuracy of the stick model. But the fact that the stick model is always generated along the structural elastic axis which is deviated from the structural layout coordinate reduces the accuracy of the stick model. Trying to generate the stick model to have a similar orientation of the wing layout coordinate system generates a discontinuous series of beam elements because the stick model should be generated within the envelope of the wing.

In this paper, we propose a new methodology to extract the stiffness properties of cantilevered complex structures with respect to any assumed coordinate system. A 3-D FEM of the main structure is the platform of our analysis. The method is validated by generating the stick model of the DLR-F6 wing 3-D FEM. The static deformations experienced by the 3-D FEM and the stick model generated by the proposed methodology and other methodologies used in the industry are presented and compared. The results obtained from our stick model are in good agreement with those of the 3-D FEM. The results show the simplicity and the accuracy of the new methodology.

II. Proposed Methodology

In this study a methodology to develop an accurate and efficient stick model is presented for a simple beam element. The methodology is then employed to extract the stick model of the DLR-F6 aircraft's wing box.

Consider the fixed-free beam element shown in Fig. 2. The principal coordinate system O_p is located at the centroid of the fixed end cross-section area. Axes x_p and z_p present the beam bending principal axes and y_p is its torsional principal axis.

The second moment of inertia of this beam around the x_p axis can be easily determined by applying a unit moment at its tip (free end) around the x_p axis and calculating the corresponding angle of rotation θ_{x_p}. Then, the principal moment of inertia around the x_p axis can be easily calculated as

$$I_{x_p} = \frac{1}{E}\frac{L}{|\theta_{x_p}|} \tag{1}$$

We emphasize here the simple fact that applying a moment around a principal axis does not generate any coupled deformations, that is, the only deformation encountered here is around the x_p axis.

Similarly, the principal moment of inertia around the y_p and z_p axes can be calculated as

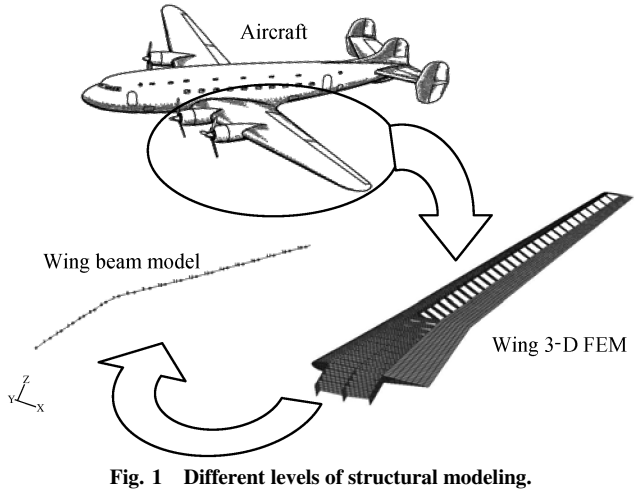

Fig. 1 Different levels of structural modeling.

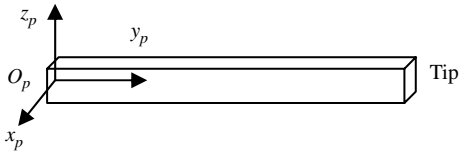

Fig. 2 Schematic drawing of a fixed-free beam element.

$$I_{z_p} = \frac{1}{E}\frac{L}{|\theta_{z_p}|} \tag{2}$$

$$I_{y_p} = \frac{1}{G}\frac{L}{|\theta_{y_p}|} \tag{3}$$

where G and E are the beam material shear and elasticity modulii, respectively, L is the length of the beam element, and θ_{y_p} and θ_{z_p} are the deformation rotational angles around y_p and z_p axes, respectively, due to unit moments.

Now, another analysis coordinate system o'_p with axes (x, y_p, z) shown in Fig. 3 is considered where x and z are two general bending axes while the torsional axis is maintained as principal.

In this case, a moment around the x axis (M_x) or around the z axis (M_z) generates rotations around both x and z axes as x and z are not principal axes. Thus we can write [17]

$$M_x = \frac{E}{L}(\theta_x I_x + \theta_z I_{xz}) \tag{4}$$

$$M_z = \frac{E}{L}(\theta_z I_z + \theta_x I_{xz}) \tag{5}$$

where I_{xz} is the product moment of inertia. Applying a unit bending moment around the x axis ($M_x = 1,\ M_y = 0,\ M_z = 0$) and considering Eqs. (4) and (5) results in

$$1 = \frac{E}{L}(\theta_x I_x - \theta_z I_{xz}) \tag{6a}$$

$$0 = \frac{E}{L}(-\theta_z I_z + \theta_x I_{xz}) \tag{6b}$$

The negative sign in the θ_z angle is due to the fact that a positive moment around the x axis generates a negative rotation angle around the z axis. Coupling Eqs. (6a) and (6b) results in

$$\frac{L}{E\theta_z} = \frac{\theta_x}{\theta_z} I_x - \frac{\theta_z}{\theta_x} I_z \tag{7}$$

Similarly applying a unit moment around the z axis ($M_x = 0$, $M_y = 0$, $M_z = 1$) and considering Eqs. (4) and (5) results in

$$0 = \frac{E}{L}(-\theta'_x I_x + \theta'_z I_{xz}) \tag{8a}$$

$$1 = \frac{E}{L}(\theta'_z I_z - \theta'_x I_{xz}) \tag{8b}$$

Coupling Eqs. (8a) and (8b) results in

$$\frac{L}{E\theta'_x} = -\frac{\theta'_x}{\theta'_z} I_x + \frac{\theta'_z}{\theta'_x} I_z \tag{9}$$

Solving Eqs. (7) and (9) simultaneously, results in

$$I_x = \frac{L}{E}\left[\frac{\left(\frac{\theta'_z}{\theta'_x\theta_z} + \frac{\theta_z}{\theta_x\theta_z}\right)}{\left(\frac{\theta'_z\theta_x}{\theta'_x\theta_z} - \frac{\theta'_x\theta_z}{\theta'_z\theta_x}\right)}\right] \tag{10a}$$

$$I_z = \frac{L}{E}\left[\frac{\left(\frac{\theta'_x}{\theta'_z\theta_z} + \frac{\theta_x}{\theta_x\theta_z}\right)}{\left(\frac{\theta'_z\theta_x}{\theta'_x\theta_z} - \frac{\theta'_x\theta_z}{\theta'_z\theta_x}\right)}\right] \tag{10b}$$

$$I_{xz} = \frac{L}{E}\left[\frac{\left(\frac{1}{\theta_z} + \frac{\theta_z}{\theta'_z\theta_x}\right)}{\left(\frac{\theta'_x\theta_x}{\theta'_x\theta_z} - \frac{\theta'_x\theta_z}{\theta'_z\theta_x}\right)}\right] \tag{10c}$$

The torsional stiffness can be calculated using Eq. (3), as the torsional axis remains principal in this case. It is worth mentioning here that the previous analysis is based on a simple beam theory, where Euler–Bernoulli beam assumptions are presumed.

The basic function of the stick model is to present accurate predictions of the real structure deformations when it is subjected to similar loading. It is basically used in the multidisciplinary design optimization algorithm to calculate the convergence of the aerodynamic loads before passing the load case to the real structural optimization algorithm to optimize the structural variables. Based on that, at a specific wing station, under the same loading, the shear center of the real structure and the corresponding point on the stick model should deform to the same coordinate in the space. This property can be enforced using a 3-D rigid body transformation. Then, a correction factor is generated to modify the rigid body deformation to the elastic deformations. This process is explained next.

Let us consider a beam element in which none of its principal axes is known. Instead an arbitrary analysis coordinate system with any defined orientation is assumed. As shown in Fig. 4, a general analysis coordinate system O, in which none of its axes (x, y, z) is a principal axis, is defined. In other words, a moment applied on the beam in Fig. 4 around the x axis will generate deformation rotational angles around the x, y, and z axes.

Applying a moment M_x around the x axis at the tip of the beam shown in Fig. 4 causes the tip to experience three rotational deformations of θ_x, θ_y, and θ_z. Assume that the undeformed coordinate of the tip point of the beam in Fig. 4 with respect to coordinate system O is (x_t, y_t, z_t); then its new coordinate after deformation may be obtained as

$$\begin{bmatrix} x'_t \\ y'_t \\ z'_t \end{bmatrix} = C * \begin{bmatrix} 1 & 0 & 0 \\ 0 & \cos(\theta_x) & -\sin(\theta_x) \\ 0 & \sin(\theta_x) & \cos(\theta_x) \end{bmatrix} * \begin{bmatrix} \cos(\theta_y) & 0 & \sin(\theta_y) \\ 0 & 1 & 0 \\ -\sin(\theta_y) & 0 & \cos(\theta_y) \end{bmatrix} * \begin{bmatrix} \cos(\theta_z) & -\sin(\theta_z) & 0 \\ \sin(\theta_z) & \cos(\theta_z) & 0 \\ 0 & 0 & 1 \end{bmatrix} * \begin{bmatrix} x_t \\ y_t \\ z_t \end{bmatrix} \tag{11}$$

where C is a correction factor to evaluate elastic deformations based on rigid body deformations. This correction factor is found to be 0.5. To illustrate this, let us examine a special case with principal coordinate axes as shown in Fig. 2. Using a simple beam theory, it is well known that applying a moment M around the x_p axis at the tip of

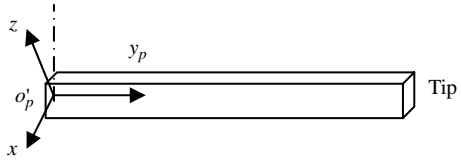

Fig. 3 Schematic drawing of a fixed-free beam element with a coordinate system (two general bending axes and a principal torsional axis) attached at the centroid of the fixed end.

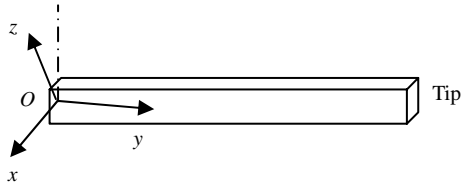

Fig. 4 Schematic drawing of a fixed-free beam element with a general coordinate system attached at the centroid of the fixed end.

an elastic beam yields the following tip displacement along the z_p axis:

$$z_p(L) = \frac{1}{2}\frac{ML^2}{EI_{x_p}} \tag{12}$$

Because the x_p axis is a principal axis, the centroid of the tip will experience only rotation angle θ_{x_p} as the 3 rotational degrees of freedom of the tip grid point are decoupled with respect to the assumed analysis principal coordinate system. If a point p on the z_p–y_p plane with coordinate (x_p, y_p, z_p) experiences a rotation θ_{x_p} around the x axis, the new coordinate (x'_p, y'_p, z'_p) can be obtained from simple transformation as

$$\begin{bmatrix} x'_p \\ y'_p \\ z'_p \end{bmatrix} = \begin{bmatrix} 1 & 0 & 0 \\ 0 & \cos(\theta_{x_p}) & -\sin(\theta_{x_p}) \\ 0 & \sin(\theta_{x_p}) & \cos(\theta_{x_p}) \end{bmatrix} \begin{bmatrix} x_p \\ y_p \\ z_p \end{bmatrix} \tag{13}$$

If the point p is located at the centroid of the cross section of the beam tip, in Fig. 2, then ($x_p = z_p = 0$ and $y_p = L$); then after a rotation of θ_{x_p}, the new coordinates can be calculated as

$$\begin{bmatrix} x'_p \\ y'_p \\ z'_p \end{bmatrix} = \begin{bmatrix} 1 & 0 & 0 \\ 0 & \cos(\theta_{x_p}) & -\sin(\theta_{x_p}) \\ 0 & \sin(\theta_{x_p}) & \cos(\theta_{x_p}) \end{bmatrix} \begin{bmatrix} 0 \\ L \\ 0 \end{bmatrix} \tag{14}$$

For small rotation angles, $\cos(\theta_{x_p}) \approx 1$ and $\sin(\theta_{x_p}) \approx \theta_{x_p}$, then, a change in the point location along the z_p axis can be expressed as

$$z'_p(L) = \theta_{x_p} L \tag{15}$$

where the angle θ_{x_p} can be expressed as

$$\theta_{x_p} = \frac{ML}{EI_{x_p}} \tag{16}$$

Substituting Eq. (16) into Eq. (15) yields

$$z'_p(L) = \frac{ML^2}{EI_{x_p}} \tag{17}$$

Equation (17) provides the tip deflection obtained from rigid body transformation based on the elastic rotational angle induced by the moment about the x_p axis. However, Eq. (12) provides elastic deformation obtained by the Euler–Bernoulli beam theory. Now to make sure that rigid body transformation methodology produces the same elastic deformation result, the right-hand side of Eq. (17) should be multiplied by 0.5 which implies that Eq. (13) be revised as

$$\begin{bmatrix} x'_p \\ y'_p \\ z'_p \end{bmatrix} = \frac{1}{2}\begin{bmatrix} 1 & 0 & 0 \\ 0 & \cos(\theta_x) & -\sin(\theta_x) \\ 0 & \sin(\theta_x) & \cos(\theta_x) \end{bmatrix} \begin{bmatrix} x_p \\ y_p \\ z_p \end{bmatrix} \tag{18}$$

The same applies to Eq. (11) for the general case, which results in

$$\begin{bmatrix} x'_t \\ y'_t \\ z'_t \end{bmatrix} = \frac{1}{2} * \begin{bmatrix} 1 & 0 & 0 \\ 0 & \cos(\theta_x) & -\sin(\theta_x) \\ 0 & \sin(\theta_x) & \cos(\theta_x) \end{bmatrix} * \begin{bmatrix} \cos(\theta_y) & 0 & \sin(\theta_y) \\ 0 & 1 & 0 \\ -\sin(\theta_y) & 0 & \cos(\theta_y) \end{bmatrix} * \begin{bmatrix} \cos(\theta_z) & -\sin(\theta_z) & 0 \\ \sin(\theta_z) & \cos(\theta_z) & 0 \\ 0 & 0 & 1 \end{bmatrix} * \begin{bmatrix} x_t \\ y_t \\ z_t \end{bmatrix} \tag{19}$$

Assume that the beam element in Fig. 4 is replaced by a new beam element that is oriented to the shown coordinate system in such a way that the y axis presents its principal torsional axis. Applying a moment around the x axis generates three deformations to the original beam element, as previously explained, but generates only two bending deformation angles on the new beam element, as the torsional degree of freedom is decoupled from the bending degrees of freedom in the new beam element. This modifies Eq. (19) to include only two deformation angles, θ_x and θ_z, while $\theta_y = 0$. Thus Eq. (19) becomes

$$\begin{bmatrix} x'_t \\ y'_t \\ z'_t \end{bmatrix} = \frac{1}{2} * \begin{bmatrix} 1 & 0 & 0 \\ 0 & \cos(\theta_x) & -\sin(\theta_x) \\ 0 & \sin(\theta_x) & \cos(\theta_x) \end{bmatrix} * \begin{bmatrix} \cos(\theta_z) & -\sin(\theta_z) & 0 \\ \sin(\theta_z) & \cos(\theta_z) & 0 \\ 0 & 0 & 1 \end{bmatrix} * \begin{bmatrix} x_t \\ y_t \\ z_t \end{bmatrix} \tag{20}$$

Information about the undeformed coordinate of the original beam tip and its deformed coordinate enables us, using Eq. (20), to calculate the bending deformations that the new model has to experience to reach the same deformed coordinate in space similar to the original beam, under the same loading.

As previously shown, using the coordinate system where x and z are two general bending axes and y is a principal torsional axis, one can easily obtain the second and product moment of inertias using Eq. (10) provided that angles θ_x, θ_z and θ'_x, θ'_z are known. Considering two load cases of ($M_x = 1$, $M_y = 0$, $M_z = 0$) and ($M_x = 0$, $M_y = 0$, $M_z = 1$) on the beam element in Fig. 4, one can calculate the final deformed coordinate of the beam tip. Using these coordinates the bending deformation angles θ_x, θ_z and θ'_x, θ'_z of the new beam element can be computed using Eq. (20).

By a similar analogy, the same concept can be applied to the aircraft wing structure and its stick model. Let us assume that the beam element in Fig. 4 is the real structure of the aircraft wing, and the task is to replace that beam element by another beam element which represents the stick model, with axis y, in Fig. 4, representing the extension of the wing elastic axis within one wing bay. Because the y axis of Fig. 4 represents the elastic axis of the wing, it is also the principal torsional axis of the stick model within that wing bay. If we have the 3-D FEM of the aircraft wing and we need to generate its stick model, we simply can define a coordinate system at each wing station with one of its axes extending along the wing elastic axis (this is considered the principal torsional axis of the stick model) and its origin is at the wing station shear center. Applying a unit moment around the defined axes enables the calculation of the wing deformed displacements. These displacements can be used in Eq. (20) to find the bending deformations of the stick model which can be used in Eq. (10) to calculate the stick model equivalent bending stiffnesses. It should be noted that the proposed methodology modifies the extraction process of the bending stiffness of the stick model while the torsional stiffness is predicted using the approximated methodology presented in [1,2]. The proposed methodology to predict the bending stiffnesses will be shown to enhance the final performance of the stick model significantly.

III. Validation of the Proposed Methodology

To validate the new methodology a 3-D FEM of the DLR-F6 wing-box structure has been created as shown in Fig. 5. The wing box of the DLR-F6 is divided into 22 stations, where a local optimization of the dimensions of the wing-box components at each wing station is conducted to size the wing box. The objective function of the optimization is the mass minimization while all other dimensions of the wing-box cross sections are related to the design variables by a set of empirical equations aimed to maximize the stiffness of the wing box [18]. The design variables of the optimization process are the skin thickness and the stringer's pitches. A set of stability and strength constraints are placed. For full details about the 3-D FEM of

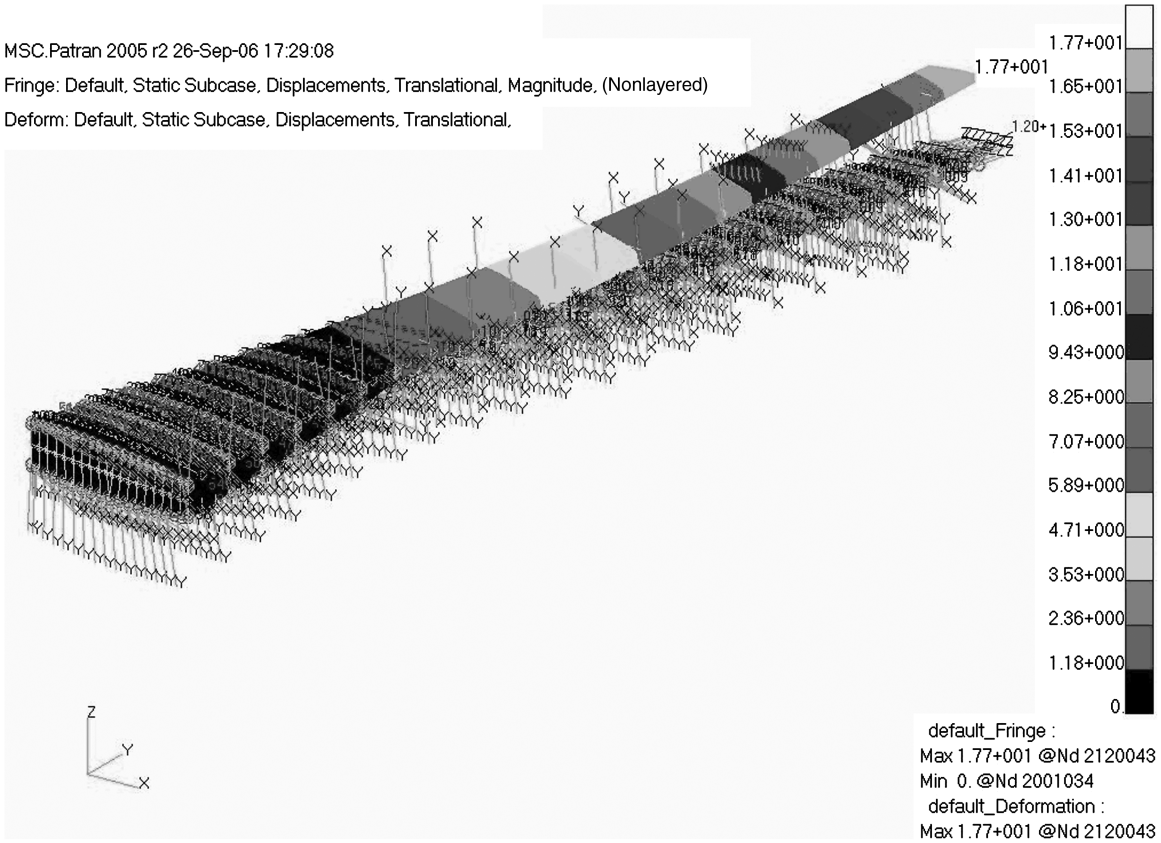

Fig. 5 3-D FEM of the DLR-F6 aircraft wing box created in PATRAN and analyzed in NASTRAN.

the DLR-F6 aircraft used in this paper and the optimization process, the reader is referred to [19].

The stick model of this 3-D FEM is generated using the methodologies available in literature as well as using the proposed methodology described in Sec. II. The performance of the generated stick models is compared with that of the 3-D FEM in the form of bending and twisting deformations with respect to the same load case, as described next.

A. Analytical Procedure to Generate Wing Stick Model (Method I)

The traditional procedure to obtain the moments of inertia of a structure is that once the wing's layout and structural details are obtained, the wing cross-sectional properties can be calculated analytically.

Figure 6 shows the detailed dimensions, geometry, and modeling coordinate systems of the DLR-F6 aircraft. Also it shows the geometrical points of the airfoil sections of the aircraft's left wing in its wing coordinate system. Consider the airfoil section of the wing at station j, located at an arbitrary normalized coordinate η_j along the wing span, where $\eta_j = y_j^*/s^*$, where y_j^* is the y coordinate of the jth wing station in the wing coordinate system, while s^* is the semispan of the DLR-F6 aircraft.

A wing cross section at any arbitrary wing station j is shown in Fig. 7 in which three main points are defined: namely, the quarter chord point (qc), the shear center (sc) of the airfoil cross section, and the centroid of the airfoil cross-sectional area (CG). The quarter chord point (qc) is located at a distance $c_j/4$ measured from the leading edge in the horizontal direction, where c_j is the local chord length at wing station j. Also a local coordinate system $o_{i,j}(x_{i,j}, y_{i,j}, z_{i,j})$ is defined with its origin located at the centroid of an arbitrary stringer (i) of coordinate $(\bar{X}_{i,j}^*, s^*\eta_j, \bar{Z}_{i,j}^*)$ defined in the wing coordinate system. The axes of this coordinate system are showing the principal directions of the z-shaped stringer.

Because the stringers are assumed to carry the bulk of bending in skin-stringer sections, only the areas of the stringers as shown in Fig. 7 are used in the calculation of the section centroid. Figure 8 shows different dimensions of the "Z"-type stringer.

The wing cross-sectional inertia properties can easily be determined with respect to the coordinate system located at the centroids of each section and parallel to the wing layout coordinate system. Also the cross-section area of the wing box at each station can easily be calculated.

The shear factors considered for the shear deformations in the wing box are calculated using the following relations [20]:

$$K_z = \int_A \frac{S_x^2 A}{I_x^2 b^2}\,\mathrm{d}A \quad \text{and} \quad K_x = \int_A \frac{S_z^2 A}{I_z^2 b^2}\,\mathrm{d}A \tag{21}$$

where S is the static moment of the cross-sectional area above the principal axis perpendicular to the direction of the shear deformation, A is the cross-section area of the wing-box station, while b is the breadth at the centroid.

It should be noted that there is an approximation in this analytical methodology as it is assumed that the orientation of the stick model beam element is in the same direction as the orientation of the wing layout coordinate system which is not accurate. The reason is that the taperness in the different parts of the wing box, the dihedral angle, and the twisted geometry of the wing prevent the coincidence between the elastic axis and the wing layout torsional axis. This will cause coupling between the torsional degrees of freedom and the 2 bending degrees of freedom which subsequently generate errors.

The cross-sectional properties of the DLR-F6 aircraft wing box along the wing span are calculated analytically and provided in Table 1.

NASTRAN Implementations: The stick model of the aircraft wing box at each wing bay is modeled by a beam element along the bay elastic axis with approximate beam properties at the two stations of that particular bay as shown in Fig. 9. The stiffness properties of the element at each bay section are extracted from Table 1 to generate the property cards required as an input in NASTRAN.

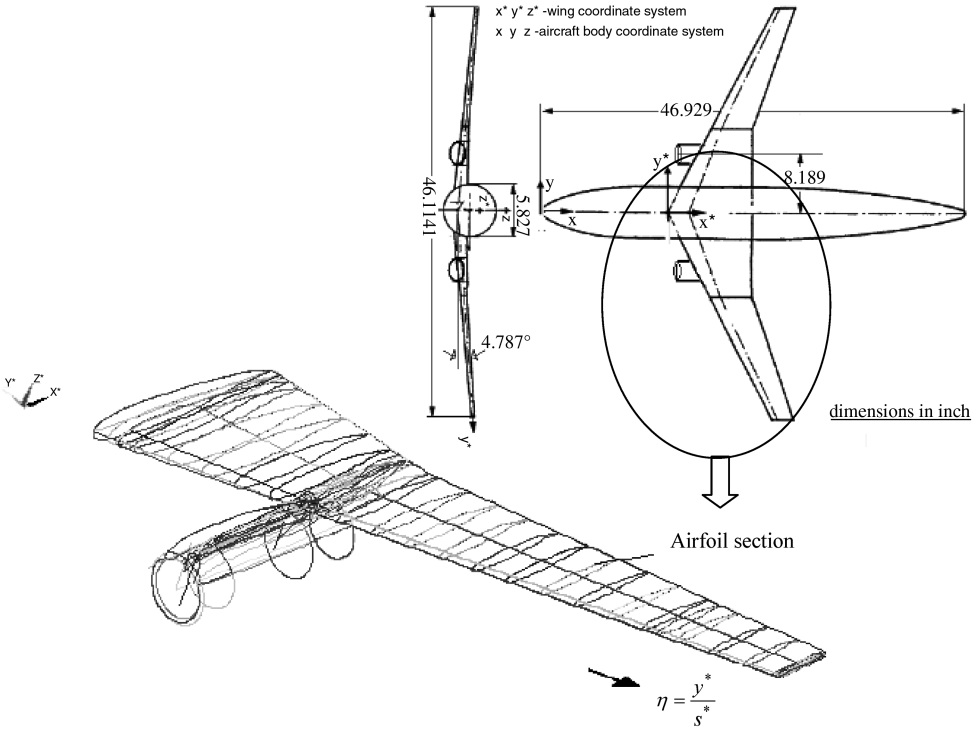

Fig. 6 Detailed dimensions and geometry of the DLR-F6 aircraft along with its wing showing different airfoil sections [22].

Any kind of loading can be used to test the accuracy of the stick model, but to be realistic, a load case of critical cruising conditions generated by the computational fluid dynamics solution for the wing–body–pylon–engine (wind mounted engine) case giving the lift coefficient and pitching moment coefficient for the DLR-F6 aircraft wing at test conditions of Mach number 0.75, overall lift coefficient 0.5, dihedral angle of −0.0111 deg, Reynolds number of 0.3E7, and altitude of 50,000 ft is used to test the accuracy of the stick model.

The horizontal, twisting angle and vertical deformations of the generated analytical stick model are compared with those obtained from the 3-D FEM for the same load case, as shown in Figs. 10–12. It should be noted that the deformations obtained in this paper are simply based on linear static analysis and no static aeroelastic analysis has been conducted.

As it can be realized, the results obtained from the stick model generated based on the analytical analysis are not in good agreement with those obtained by the 3-D FEM. This is mainly due to the fact that the torsional principal axis of the beam elements used to generate the stick model does not coincide with the wing torsional coordinate of the wing layout which is the orientation used in the analytical methodology to calculate the wing stiffness properties.

B. Wing Stick Model Extracted from the Full 3-D FEM (Method II)

The second methodology extracts the stiffness properties of the beam model from the complete 3-D FEM of the wing box. The method requires some processing in PATRAN and NASTRAN [18] and it requires that the user be knowledgeable of both software packages. The method assumes that the stiffness extraction process begins by locating the shear center at each wing station where a local coordinate system is created along the elastic axis as well as the axes of the principal inertia. The limitation of this methodology is its dependency on the principal directions to create the analysis coordinate system, which cannot be created unless an approximation is applied. This may generate undesirable results in some cases.

1. *Equivalent Moments of Inertia of the Wing Box*

Because this methodology assumes that the stiffness properties will be generated along the principal axes, Eqs. (1–3) can be used to find the following moment of inertias [18]:

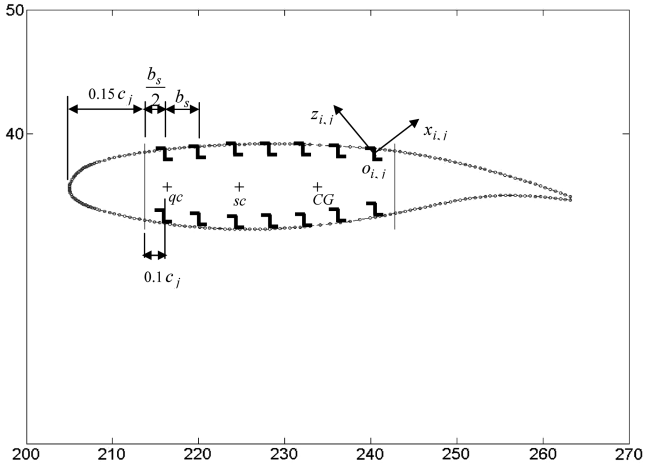

Fig. 7 Wing cross section at an arbitrary wing station *j*.

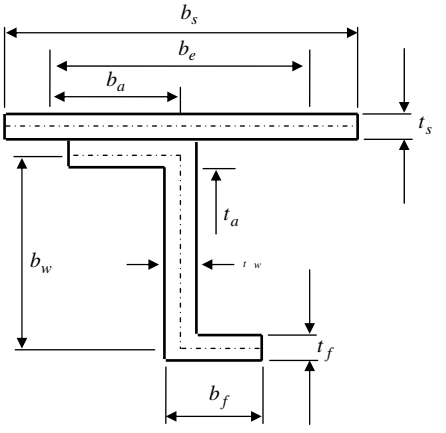

Fig. 8 Stiffened panel geometry definition using a Z-type stringer.

Table 1 Analytical calculations of cross-section properties along the DLR-F6 aircraft wing box

Station	Ix, in.^{4}	Iz, in.^{4}	I_y, in.^{4}	Ixz, in.^{4}	A, in.^{2}	K_z	K_x
1	4.2767e3	3.4059e4	38e3	−2.8803e3	31.0	0.211	1.01
2	3.2794e3	2.8709e4	31e3	−2.1267e3	30.1	0.252	1.012
3	2.5021e3	2.3969e4	25e3	−1.5271e3	29.5	0.233	0.984
4	1.8439e3	2.0188e4	22e3	−1.0778e3	28.2	0.234	0.835
5	1.3849e3	1.7091e4	18e3	−674.1277	26.11	0.235	0.87
6	887.3440	1.2731e4	13e3	−236.1660	26.05	0.206	0.91
7	663.2558	1.1312e4	12e3	−59.1673	26.02	0.215	0.85
8	520.1212	8.6682e3	9e3	−16.3241	23.01	0.203	0.837
9	446.8150	7.5715e3	8e3	2.3469	20.9	0.207	0.831
10	371.0782	6.4595e3	6.7e3	6.6140	18.8	0.208	0.81
11	301.2099	5.2220e3	5.5e3	7.3983	16.3	0.203	0.84
12	236.3099	4.0677e3	4.2e3	4.3473	13.7	0.199	0.84
13	179.7233	2.9837e3	3e3	4.9814	11.6	0.184	0.84
14	140.4200	2.4172e3	2.5e3	12.9593	9.9	0.183	0.83
15	100.6141	1.6890e3	1.7e3	5.1014	8.9	0.182	0.83
16	77.7788	1.3394e3	1.34e3	5.1876	6.1	0.171	0.83
17	67.2339	1.1887e3	1.19e3	12.9359	5.7	0.172	0.82
18	53.4311	943.3881	0.14e3	17.6004	5.5	0.175	0.77
19	45.3523	863.1392	0.9e3	22.5334	5.2	0.183	0.76
20	35.0668	666.8249	0.7e3	23.9796	4.8	0.171	0.71

$$(I_x)_{i\to j} = \frac{1}{E}\left|\frac{(\eta_j - \eta_i)S^*}{(\theta_{x_j} - \theta_{x_i})}\right| \tag{22}$$

$$(J_y)_{i\to j} = \frac{1}{G}\left|\frac{(\eta_j - \eta_i)S^*}{(\theta_{y_j} - \theta_{y_i})}\right| \tag{23}$$

$$(I_z)_{i\to j} = \frac{1}{E}\left|\frac{(\eta_j - \eta_i)S^*}{(\theta_{z_j} - \theta_{z_i})}\right| \tag{24}$$

where η_i and η_j are the normalized station's coordinates at stations i and j, respectively, while $(I_x)_{i\to j}$, $(I_y)_{i\to j}$, and $(I_z)_{i\to j}$ are the second moments of inertia, equivalent to the bay extending between stations i and j, with respect to the x, y, and z axes, respectively.

The equivalent cross-sectional area and equivalent shear factors require further processing in NASTRAN and PATRAN which is explained in the next section.

2. Equivalent EA's and GK's of the Wing Box

To evaluate the equivalent axial stiffness, EA, and the equivalent shear stiffness, GK, of the wing box, it is necessary to evaluate the equivalent cross-section area, A, and the equivalent shear factors, K, at each wing station. The process of evaluating the distribution of equivalent area and shear factors in the spanwise direction is different from that of the bending and torsional stiffness evaluation. In this process NASTRAN is executed for three load subcases for each wing-box bay. In this process, the 3 degrees of freedom related to rotation in all skin-stringers connectivity grid points at all wing stations are frozen, while the translation degrees of freedom are kept free. The elastic axis nodes are connected to the skin-stringer connectivity grid points by RBE2 [21] elements with its dependent degrees of freedom specified at the skin and its independent degrees of freedom specified at the shear center grid points.

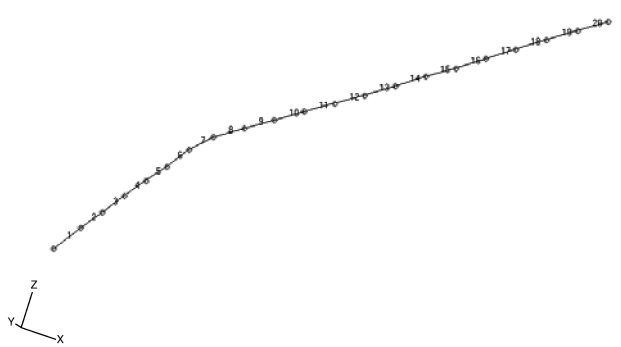

Fig. 9 DLR-F6 aircraft wing-box stick model created in NASTRAN.

In the first subcase, a unit force in the y direction (the axial direction) is applied at the bay shear center grid point, in order to calculate the equivalent area, as follows:

$$(A)_{i\to j} = \frac{1}{E}\left|\frac{(\eta_j - \eta_i)S^*}{(D_{y_j} - D_{y_i})}\right| \tag{25}$$

where $(A)_{i\to j}$ is the cross-sectional area equivalent to the bay extending between stations i and j.

In the second subcase, the structure is loaded by a unit load at the shear center in the z direction, to calculate the shear factor in the z direction as follows:

$$(K_z)_{i\to j} = \frac{1}{GA}\left|\frac{(\eta_j - \eta_i)S^*}{(D_{z_j} - D_{z_i})}\right| \tag{26}$$

Similarly, the structure is loaded by a unit force in the x direction to calculate the shear factor in the x direction, as follows;

$$(K_x)_{i\to j} = \frac{1}{GA}\left|\frac{(\eta_j - \eta_i)S^*}{(D_{x_j} - D_{x_i})}\right| \tag{27}$$

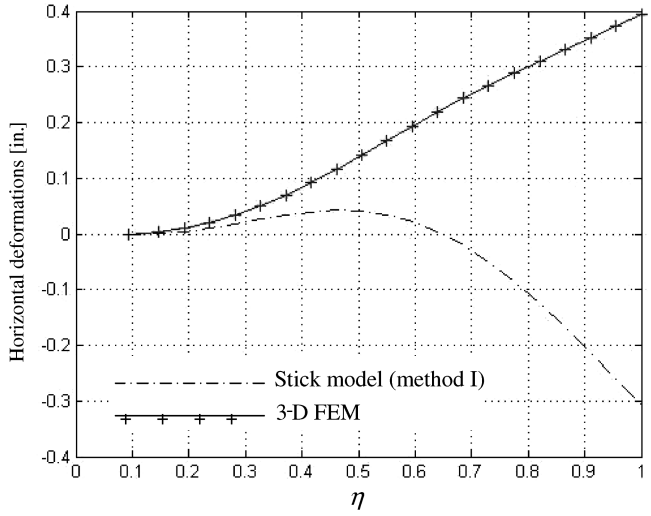

Fig. 10 Comparison between the horizontal deformation (x direction) obtained from the 3-D FEM and the stick model based on the analytical methodology.

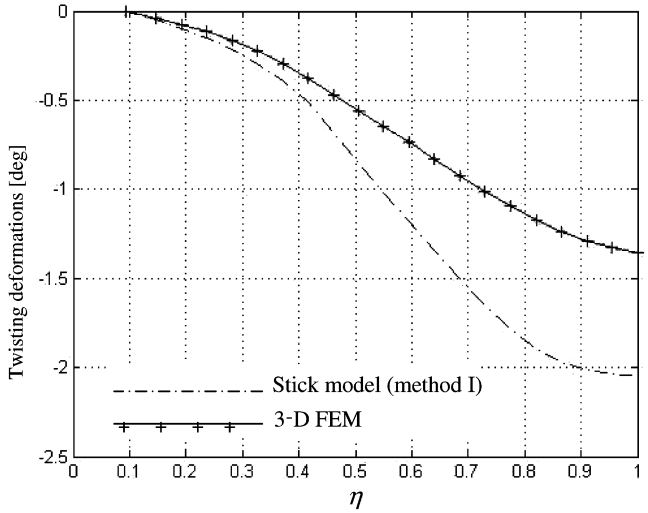

Fig. 11 Comparison between the twisting angle deformations (around *y*) obtained from the 3-D FEM and the stick model based on analytical methodology.

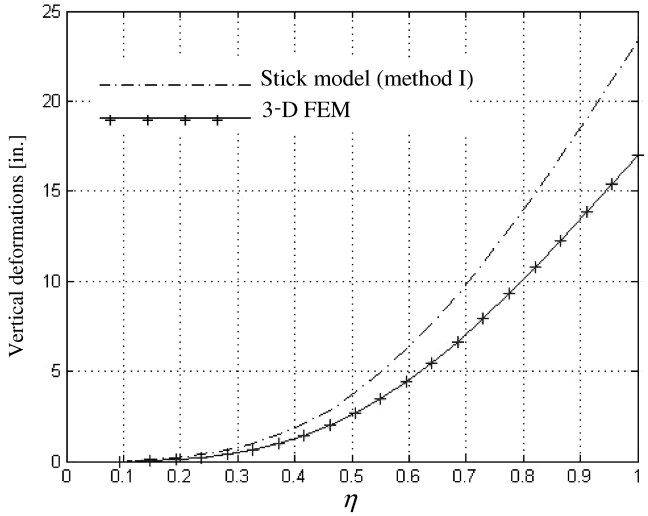

Fig. 12 Comparison between the vertical deformations (*z* direction) obtained from the 3-D FEM and the stick model based on analytical methodology.

where D denotes the displacement deformation in the relative direction. The generated equivalent moments of inertia, equivalent cross-sectional areas, and the equivalent shear factors at each wing bay are summarized in Table 2.

The stiffness properties presented in Table 2 are used to generate the stick model of the DLR-F6 wing box. The generated stick model deformations are compared with the deformations of the 3-D FEM for the same previous load case as shown in Figs. 13–15.

It can be concluded from Figs. 13–15 that the stick model generated based on the full finite element model is also not accurately representing the 3-D FEM. This is due to the approximation made to create the analysis coordinate system along the principal axes.

C. Wing Stick Model Generation Using Empirical Relations (Method III)

A methodology to estimate the stiffness distribution of a new wing using the stiffness distributions of Bombardier's existing wings was developed by Abdo et al. [6]. This methodology is based on a set of empirical relations that are generated to predict the approximate stiffness distribution of an arbitrary aircraft wing box. To obtain these empirical relations, the stiffness extraction method described in Sec. III.B has been used to extract the stiffness properties of four Bombardier wings. The results obtained are employed to obtain empirical relations that can be used to estimate the stiffness distribution of a new wing. These relations could also be used to compare the stiffness behavior of newly designed wings with the existing ones or check the stiffness predicted by other methods. To obtain the empirical relations that apply to all wings, they normalized the data to collapse the stiffness distribution of all existing wings into as tight a cloud of points as possible. Several normalization techniques were investigated [6], and the results of one of those normalization techniques were provided where the stiffness of the existing wing structure is divided by the stiffness of a solid block material bounded by the leading and trailing edge of the wing, which is referred to as $(EI)_{\text{CATIA}}$, as CATIA was used for the calculation of the wing stiffness values, as shown in Fig. 16. The empirical relations obtained are then used to generate the stiffness properties of the DLR-F6 aircraft wing box.

Figure 16 shows the airfoil sections of the DLR-F6 wing at 21 wing stations. At each wing station, the airfoil section is padded, and then the stiffness of each wing section is calculated in CATIA.

The data obtained from CATIA are used along with the empirical relations to predict the ideal stiffness properties of such aircraft wing box.

For EI_x the behavior of the normalized stiffness appeared to be different outboard and inboard of the break in the planform. Consequently, different relations were used to fit the data on the inboard and outboard wings. The final empirical relation for the normalized stiffness is as follows [6]:

$$\frac{(EI_x)_{\text{FEM}}}{(EI_x)_{\text{CATIA}}} = \frac{R_{\text{Break}} - R_{\text{Root}}}{\eta_{\text{Break}} - \eta_{\text{Root}}}(\eta - \eta_{\text{Root}}) + R_{\text{Root}} \quad \text{for } \eta_{\text{Root}} \le \eta \le \eta_{\text{Break}}$$

$$\frac{(EI_x)_{\text{FEM}}}{(EI_x)_{\text{CATIA}}} = R_{\text{Break}} \quad \text{for } \eta_{\text{Break}} \le \eta \le 1 \tag{28}$$

where

$$\eta_{\text{Break}} = \frac{y_{\text{Break}}}{S^*} \tag{29}$$

$$\eta_{\text{Root}} = \frac{y_{\text{Root}}}{S^*} \tag{30}$$

where R_{Root} is the $(EI_x)_{\text{FEM}}/(EI_x)_{\text{CATIA}}$ ratio at $\eta = \eta_{\text{Root}}$, and R_{Break} is the $(EI_x)_{\text{FEM}}/(EI_x)_{\text{CATIA}}$ ratio at $\eta = \eta_{\text{Break}}$. It was determined that $R_{\text{Root}} = 0.03$ and $R_{\text{Break}} = 0.1$ provides an acceptable fit for all airplanes.

Table 2 DLR-F6 aircraft wing-box properties generated by method II

Bay	I_x, in.^{4}	I_y, in.^{4}	I_z, in.^{4}	A, in.^{2}	K_z	K_x
1	4.2220e3	2.5894e4	1.0549e4	31.0505	0.2303	1.0244
2	3.3290e3	2.1679e4	0.8692e4	31.1960	0.2423	1.0150
3	2.5298e3	1.6881e4	0.6786e4	29.5022	0.2374	0.9807
4	1.9032e3	1.3030e4	0.5353e4	28.3718	0.2356	0.8337
5	1.3495e3	0.8151e4	0.3961e4	26.8366	0.2311	0.8602
6	1.0322e3	0.7390e4	0.3099e4	26.9245	0.221	0.8203
7	0.7285e3	0.5305e4	0.2335e4	26.2704	0.2190	0.8243
8	0.5558e3	0.4432e4	0.1774e4	23.3872	0.2048	0.8379
9	0.4592e3	0.3676e4	0.1477e4	20.9122	0.2075	0.8386
10	0.3814e3	0.3013e4	0.1213e4	18.8147	0.2056	0.8344
11	0.3071e3	0.2379e4	0.0958e4	16.3768	0.2014	0.8366
12	0.2367e3	0.1741e4	0.0716e4	13.7504	0.1935	0.8411
13	0.1850e3	0.1356e4	0.0553e4	11.6117	0.1879	0.8454
14	0.1440e3	0.1059e4	0.0431e4	9.9506	0.1890	0.8389
15	0.1156e3	0.0841e4	0.0348e4	8.9070	0.1827	0.8357
16	0.0812e3	0.0576e4	0.0233e4	6.8692	0.1792	0.8333
17	0.0610e3	0.0434e4	0.0177e4	5.7850	0.1788	0.8280
18	0.0497e3	0.0347e4	0.0145e4	5.3652	0.1790	0.7729
19	0.0406e3	0.0280e4	0.0119e4	5.0415	0.1814	0.7679
20	0.0329e3	0.0224e4	0.0098e4	4.9649	0.1728	0.7155

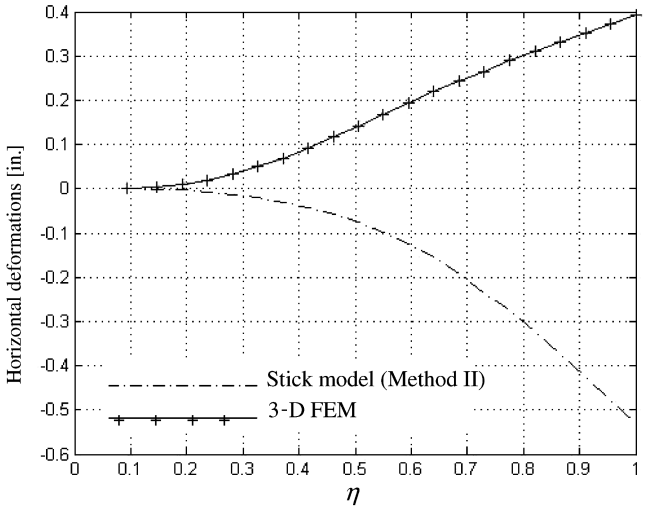

Fig. 13 Comparison between the horizontal deformations (x direction) obtained from the 3-D FEM and the stick model based on the FEM model.

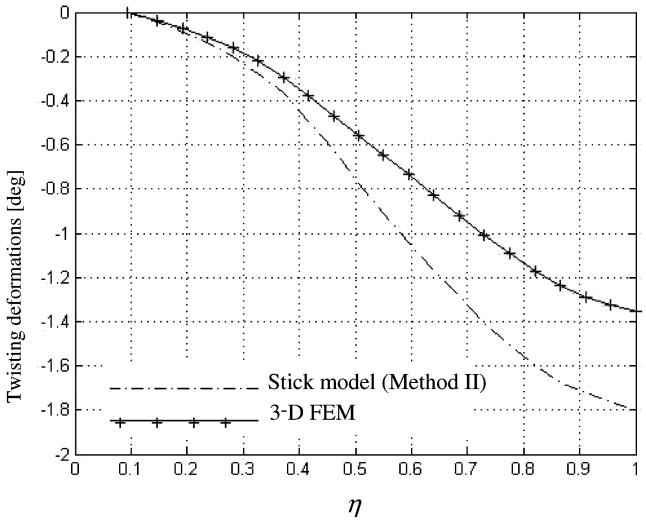

Fig. 14 Comparison between the twisting angle deformations (around y) obtained from the 3-D FEM and the stick model based on the FEM model.

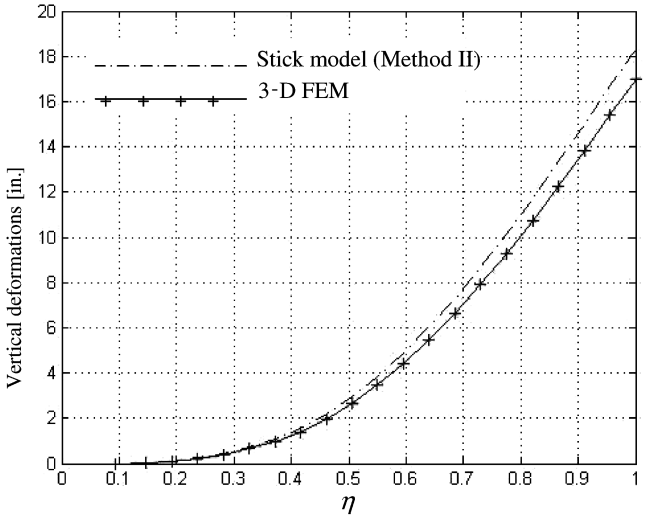

Fig. 15 Comparison between the vertical deformations (z direction) obtained from the 3-D FEM and the stick model based on the FEM model.

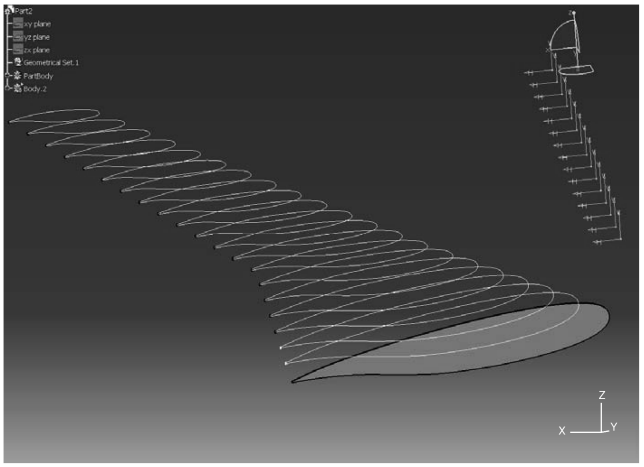

Fig. 16 DLR-F6 wing airfoil sections created in CATIA.

For GI_y the following empirical relations were developed:

$$\frac{(GI_y)_{\text{FEM}}}{(GI_y)_{\text{CATIA}}} = 0.002 \tag{31}$$

For EI_z and the cross-sectional areas the following empirical relations were developed:

$$\frac{(EI_z)_{\text{FEM}}}{(EI_z)_{\text{CATIA}}} = 0.0103\eta + 0.007 \tag{32}$$

$$\begin{aligned} \frac{(A)_{\text{FEM}}}{(A)_{\text{Airfoil}}} &= 0.1579\eta^2 - 0.0136\eta + 0.0143 \quad \text{for } 0 \le \eta < 0.65 \\ \frac{(A)_{\text{FEM}}}{(A)_{\text{Airfoil}}} &= 0.1957\eta^2 - 0.481\eta + 0.302 \quad \text{for } 0.65 \le \eta \le 1 \end{aligned} \tag{33}$$

The previous empirical relations are used to predict the stiffness properties of the DLR-F6 aircraft wing box. For the shear factors, the results obtained using method II are used to complete the entries to the beam element cards in NASTRAN because there are no empirical relations available to predict shear factors.

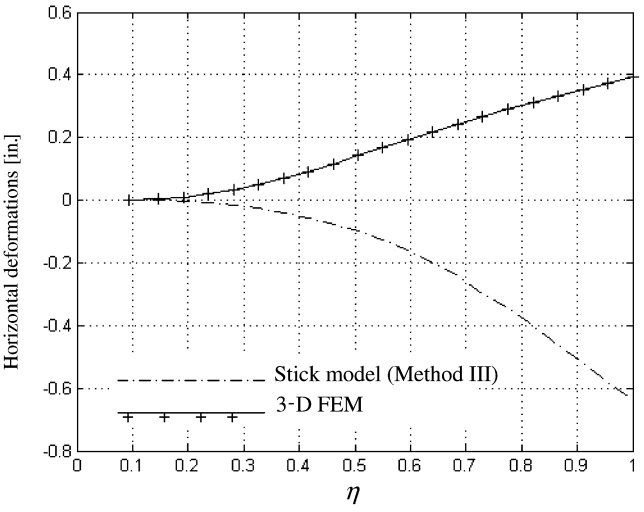

Fig. 17 Comparison between the horizontal deformations (x direction) obtained from the 3-D FEM and the stick model based on the empirical relation.

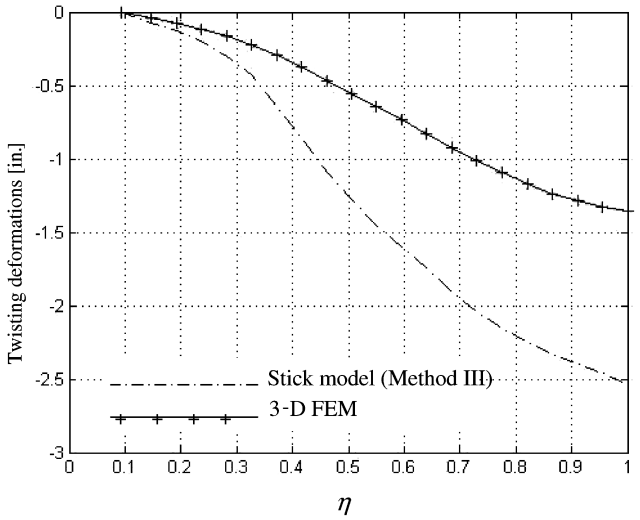

Fig. 18 Comparison between the twisting angle deformations (around *y*) obtained from the 3-D FEM and the stick model based on the empirical relation.

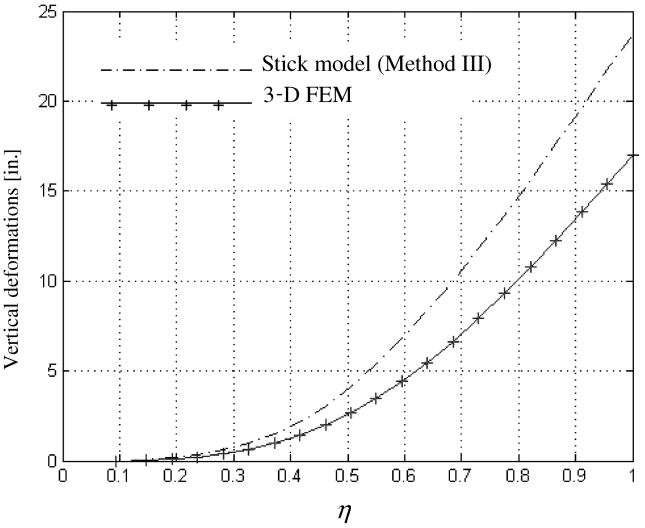

Fig. 19 Comparison between the vertical deformations (z direction) obtained from the 3-D FEM and the stick model based on the empirical relation.

The generated stick model twisting angle and horizontal and vertical deformations are compared with the 3-D FEM for the same previous load case as shown in Figs. 17–19.

As it can be seen, the empirical formulations are not accurately predicting the wing's deformations in comparison to the 3-D FEM as well. The reason is that the empirical formulas are generated based on the stiffness properties of the aircrafts extracted using method II which has its own approximation. Accumulation of approximations decreases the accuracy of the results obtained which can be concluded from Figs. 10–15 and 17–19.

D. Wing Stick Model Generated Using the Proposed Methodology (Method IV)

The proposed methodology explained in Sec. II is used to generate the stiffness properties of the DLR-F6 aircraft wing box using the developed 3-D FEM. The process needs some processing in NASTRAN and PATRAN. Each wing bay is modeled by one beam element extending along its elastic axis. The steps of extracting the stiffness properties of each wing bay can be summarized as follows:

1) As shown in Fig. 20, a local coordinate system is created with its origin located at the shear center of the wing bay station toward the tip. The z axis of this local coordinate system is placed along the elastic axis of the wing bay while the x axis is located horizontally in the chordwise direction and the y axis is automatically generated in the up direction perpendicular to the other two axes.

2) All the grid points at the bay station toward the wing root are fixed. These include the grid points perpendicular to the assumed torsional axis (the elastic axis) and the grid points in the assumed bending plane (x–y plane).

3) The analysis coordinate system of the shear center grid point of the bay station toward the tip is modified to be the local coordinate system generated in step one, so the deformation angles experienced by the shear center grid point can be retrieved in the proposed local coordinate system.

4) Two load subcases of unit moments around the x and y axes are created in NASTRAN.

5) The structural deformations encountered by the shear center grid point at the wing station toward the tip due to applying the unit moment around the x axis are obtained which are denoted by θ_x, θ_y, and θ_z in Eq. (10). It should be realized here that there is a full coupling between the 3 rotational degrees of freedom of the system.

6) To find the deformations that the equivalent system (the stick model) will experience under the same loading, one must equate Eq. (20) to Eq. (11), which enables the calculation of the two angles θ_x and θ_y. One should realize that this step implies a decoupling between the torsional degree of freedom and the 2 bending degrees of freedom while the 2 bending degrees of freedom remain coupled as discussed in Sec. II.

7) In the same manner, by applying the second load case, and finding the corresponding deformations, one can calculate the other two bending angles θ'_x and θ'_y.

8) The four deformation angles θ_x, θ_y, θ'_x, and θ'_y can now be used to calculate I_x, I_y, and I_{xy} using Eq. (10).

9) To calculate the equivalent cross-sectional area A and the two area shear factors K_1 and K_2, one can use the same methodology defined in Sec. III.B.2 taking into account the analysis coordinate system defined in step 1.

The sectional properties obtained using the proposed approach are summarized in Table 3.

These sectional properties are employed to generate the stick model. The performance of this stick model is compared with the

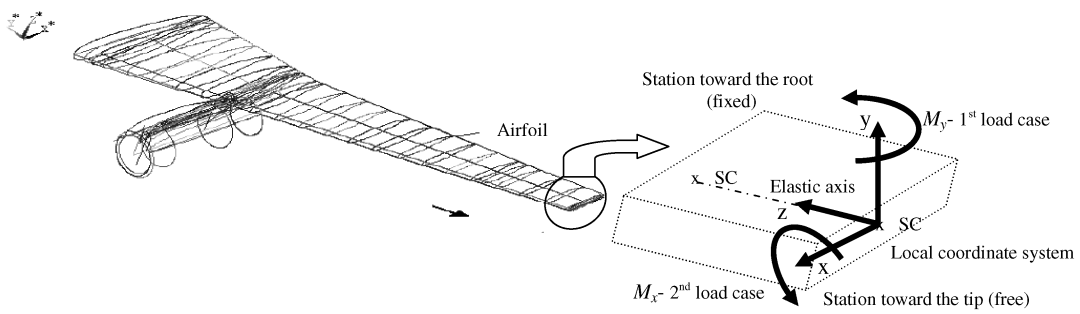

Fig. 20 Schematic drawing of one wing bay in the DLR-F6 wing with its elastic axis and local coordinate system defined to extract its stiffness properties using the new methodology. SC: shear center.

Table 3 Sectional properties of the DLR-F6 wing box extracted using method IV

Bay	I_x, in.^{4}	I_y, in.^{4}	I_z, in.^{4}	I_{xy}, in.^{4}	A, in.^{2}	K_y	K_x
1	6.4459e3	3.3682e4	4.0128e4	−5.1023e3	4.6286e1	0.15273	0.54340
2	4.8661e3	2.8821e4	3.3687e4	−4.0291e3	4.5083e1	0.16581	0.54752
3	3.5989e3	2.3657e4	2.7256e4	−3.0167e3	4.2674e1	0.16231	0.54802
4	2.6330e3	1.9530e4	2.2163e4	−2.2158e3	4.0825e1	0.16191	0.54730
5	1.6750e3	1.5627e4	1.7302e4	−8.9016e2	3.7393e1	0.16499	0.59805
6	2.6318e3	1.1176e4	1.3807e4	3.6839e3	3.2634e1	0.19079	0.56987
7	9.4449e2	1.0636e4	1.1581e4	−6.3648e2	3.8255e1	0.14898	0.53243
8	7.6597e2	8.2006e3	8.9666e3	−4.8764e2	3.2187e1	0.14803	0.57027
9	6.3685e2	6.9971e3	7.6340e3	−4.1283e2	2.9415e1	0.14672	0.55611
10	5.2715e2	5.9276e3	6.4548e3	−3.3987e2	2.6813e1	0.14346	0.54531
11	6.8708e2	6.1681e3	6.8552e3	−8.3770e2	3.3404e1	0.09848	0.40342
12	3.2606e2	3.7539e3	4.0800e3	−1.9538e2	2.0101e1	0.13174	0.53482
13	2.5122e2	2.8852e3	3.1364e3	−1.5099e2	1.7108e1	0.12674	0.53273
14	1.9586e2	2.3165e3	2.5124e3	−1.1977e2	1.4965e1	0.12488	0.51638
15	1.5540e2	1.8722e3	2.0276e3	−8.9971e1	1.3489e1	0.11989	0.51073
16	1.0962e2	1.3451e3	1.4547e3	−6.6677e1	1.0687e1	0.11441	0.49429
17	8.2216e1	1.0331e3	1.1153e3	−4.5459e1	9.2060	0.12074	0.48233
18	6.7170e1	8.5472e2	9.2189e2	−3.1691e1	8.6849	0.11776	0.47454
19	5.5144e1	7.3826e2	7.9341e2	−2.1855e1	8.4451	0.11566	0.45627
20	4.3715e1	6.1898e2	6.6269e2	−1.1611e1	7.9225	0.11669	0.45498

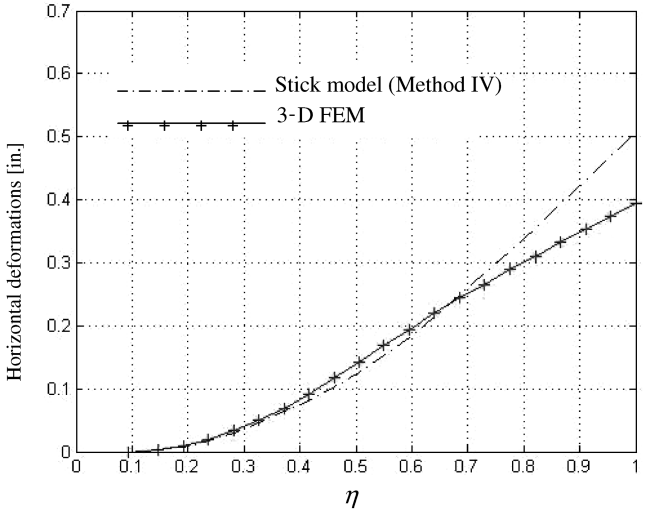

Fig. 21 Comparison between the horizontal deformations (x direction) obtained from the 3-D FEM and the stick model based on the proposed methodology.

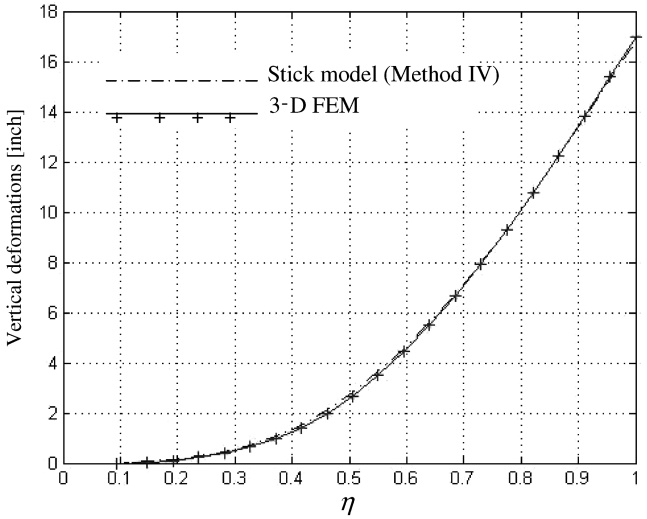

Fig. 23 Comparison between the vertical deformations (z direction) obtained from the 3-D FEM and the stick model based on the proposed methodology.

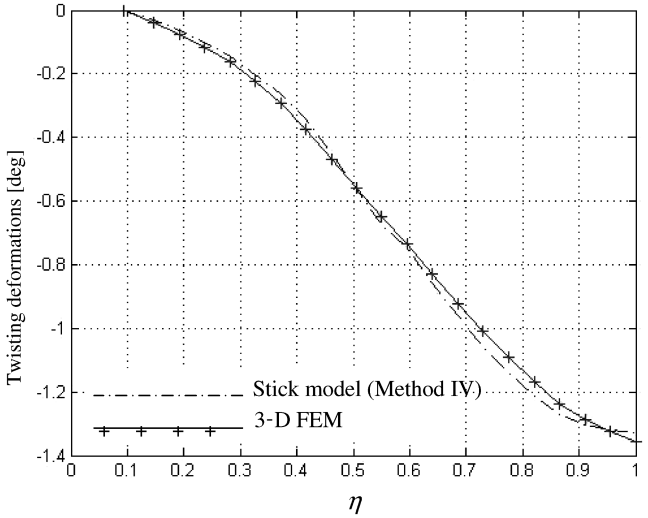

Fig. 22 Comparison between the twisting angle deformations (around y) obtained from the 3-D FEM and the stick model based on the proposed methodology.

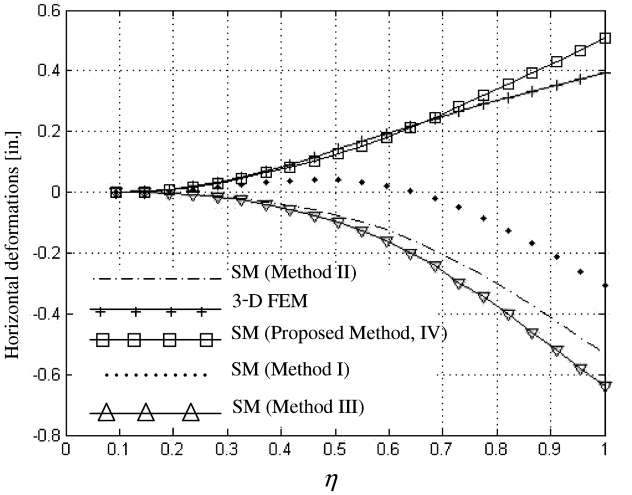

Fig. 24 Comparison between the horizontal deformations (x direction) obtained from the 3-D FEM and the stick models (SM) based on methods I–IV.

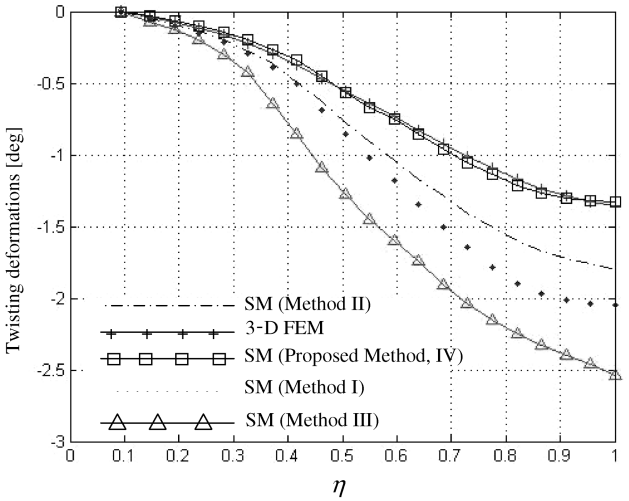

Fig. 25 Comparison between the twisting angle deformations (around y) obtained from the 3-D FEM and the stick models based on methods I–IV.

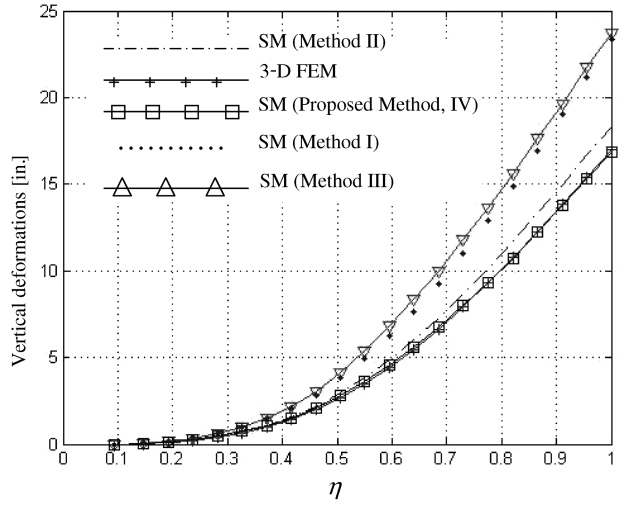

Fig. 26 Comparison between the vertical deformations (z direction) obtained from the 3-D FEM and the stick models based on methods I–IV.

performance of the 3-D FEM for the same previous load case, as shown in Figs. 21–23.

As it can be realized excellent agreement exists between the twisting angle and vertical deformation obtained from the stick model generated based on the proposed approach and those obtained from the 3-D FEM. It is interesting to note that horizontal deformation evaluated based on methods I–III does not agree at all with that based on the 3-D FEM as shown in Figs. 10, 13, and 17; however, as it can be seen from Fig. 21, the horizontal deformation obtained from the stick model based on the proposed approach is in good agreement with that of the 3-D FEM.

E. Comparison Between the Performance of the Stick Models Generated by the Different Methodologies and the 3-D FEM

For the sake of easy comparison, deformations evaluated by stick models based on methods I–III and the proposed stick model (method IV) and also the results obtained by full 3-D FEM are shown in Figs. 24–26.

As it can be realized from Figs. 24–26 the results obtained from the stick model generated by the proposed methodology are in very good agreement with those of the full 3-D FEM, thus confirming its high accuracy. The model is efficient and accurate enough to be used in static aeroelastic analysis.

IV. Conclusions

In this paper, the process of generating a wing stick model is investigated. A new methodology for generating stick models with higher accuracy than methods available in the literature is introduced and compared with stick models generated using methodologies adopted by the industry. It has been shown that the predicted wing deformation results obtained from the stick model based on the new methodology are in good agreement with those of the full 3-D finite element model. The developed high accuracy stick model can be effectively used for static aeroelasticity, design optimization, and MDO.

Acknowledgment

Support from the Consortium for Research and Innovation in Aerospace in Quebec (CRIAQ) is gratefully acknowledged.

References

[1] Adelman, H. M., and Mantay, W. R., "Integrated Multidisciplinary Design Optimization of Rotorcraft," *Journal of Aircraft*, Vol. 28, No. 1, Jan. 1991, pp. 22–28. doi:10.2514/3.45988

[2] Adelman, H., Walsh, J., and Pritchard, J., "Recent Advances in Integrated Multidisciplinary Optimization of Rotorcraft," AIAA Paper 92-4777, 21–23 Sept. 1992.

[3] AIAA White Paper "Current State of the Art of Multidisciplinary Design Optimization," prepared by the AIAA Technical Committee for MDO, approved by AIAA Technical Activities Committee, Washington, D.C., Sept. 1991.

[4] Altus, S., Bischof, C., Hovland, P., and Kroo, I., "Using Automatic Differentiation with the Quasi-Procedural Method for Multidisciplinary Design Optimization," *34th AIAA Aerospace Sciences Conference*, AIAA, Reston, VA, 15–18 Jan. 1996.

[5] Chattopadhyay, A., and Pagaldipti, N., "A Multidisciplinary Optimization Using Semi-Analytical Sensitivity Analysis Procedure and Multilevel Decomposition," *Journal of Computers and Mathematics with Applications*, Vol. 29, No. 7, 1995, pp. 55–66.

[6] Abdo, M., L'Heureux, R., Pepin, F., and Kafyeke, F., "Equivalent Finite Element Wing Structural Models Used for Aerodynamics-Structures Intraction," *CASI 16th Aerospace Structures and Materials Symposium*, Montreal, Quebec, April 2003.

[7] Abdo, M., and Pepin, F., "Transonic Aerodynamics of Flexible Wings," *CASI 48th Annual Conferences Proceedings*, Canadian Aeronautics and Space Institute, Toronto, Ontario, 2001, pp. 47–53.

[8] Abdo, M., Piperni, P., Isikveren, A., and Kafyeke, F., "Optimization of a Business Jet," *CASI Annual General Meeting, Aircraft Design & Development Symposium*, Toronto, Ontario, April 2005.

[9] Piperni, P., Abdo, M., and Kafyeke, F., "The Building Blocks of Multi-Disciplinary Wing Design Method," *CASI 50th Annual General Meeting*, Canadian Aeronautics and Space Institute, Montreal, Quebec, 2003.

[10] Guyan, R. J., "Reduction of Stiffness and Mass Matrices," *AIAA Journal*, Vol. 13, No. 2, Feb. 1965, p. 380.

[11] Kidder, R. L., "Reduction of Structural Frequency Equations," *AIAA Journal*, Vol. 13, No. 5, 1975, p. 892.

[12] Miller, C. A., "Dynamic Reduction of Structural Models," *Journal of Structural Division, ASCE*, Vol. 106, No. 10, Oct. 1980, pp. 2097–2108.

[13] Paz, M., "Dynamic Condensation," *AIAA Journal*, Vol. 22, No. 5, 1984, pp. 724–727. doi:10.2514/3.48498

[14] *MSC/NASTRAN Application's Manual*, Vol. 1, The MacNeal-Schwendler Corporation, California, 1984.

[15] Hashemi-Kia, M., and Toossi, M., "Development and Application of a Technique for Reducing Airframe Finite Element Models for Dynamics Analysis," NASA, CR 187448, Oct. 1990, McDonnell Douglas Helicopter Company, Mesa, AZ.

[16] Kafyeke, F., Abdo, M., Pepin, F., Borowiec, Z., and Marleau, A., "Transonic Aerodynamics of Flexible Wings," *CASI 48th Annual Conference Proceedings*, Toronto, Ontario, 2001.

[17] Curtis, H. D., *Fundamentals of Aircraft Structural Analysis*, McGraw–Hill, New York, 1997.

[18] Abdo, M., Piperni, P., and Kafyeke, F., "Conceptual Design of Stringer Stiffened Compression Panels," *CASI 16th Aerospace Structures and Materials Symposium*, Montreal, Quebec, April 2003.

[19] Elsayed, M. S. A., Sing, A., and Sedaghati, R., "3D Finite Element

Model of DLR-F6 Aircraft Wing-Box Structure, Created in PATRAN and Analyzed in NASTRAN," MOSAIC Project, Rept. 6, Sponsor's Ref. No. CRIAQ 4.1-TASK 6 Sept. 2006.

[20] Orosz, I., "Simplified Method for Calculating Shear Deflections of Beams," Forest Products Laboratory, Forest Service, U.S. Department of Agriculture, FOREST SERVICE, in cooperation with the University of Wisconsin, FPL-0210, 1970.

[21] Raymond, M., and Miller, M., MSC/NASTRAN, "Quick Reference Guide" Ver. 68, 1994.

[22] *3rd AIAA CFD Drag Prediction Workshop*, AIAA, Reston, VA, 2006, http://aaac.larc.nasa.gov/tsab/cfdlarc/aiaa-dpw.

R. Ohayon
Associate Editor